Journal Pre-proof

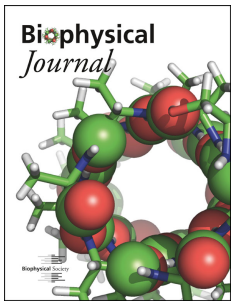

Glycogen-dependent demixing of frog egg cytoplasm at increased crowding

James F. Pelletier, Christine M. Field, Margaret Coughlin, Lillia Ryazanova, Matthew Sonnett, Martin Wühr, Timothy J. Mitchison

PII: S0006-3495(26)00495-9

DOI: https://doi.org/10.1016/j.bpj.2026.07.014

Reference: BPJ 14454

To appear in: *Biophysical Journal*

Received Date: 8 April 2026

Accepted Date: 13 July 2026

Please cite this article as: Pelletier JF, Field CM, Coughlin M, Ryazanova L, Sonnett M, Wühr M, Mitchison TJ, Glycogen-dependent demixing of frog egg cytoplasm at increased crowding, *Biophysical Journal* (2026), doi: https://doi.org/10.1016/j.bpj.2026.07.014.

Glycogen-dependent demixing of frog egg cytoplasm at increased crowding

James F. Pelletier[1,2], Christine M. Field[1,2], Margaret Coughlin[1], Lillia Ryazanova[3,4], Matthew Sonnett[1,3,4], Martin Wühr[3,4], Timothy J. Mitchison[1,2]

[1]Department of Systems Biology, Harvard Medical School, Boston, MA, USA
[2]Marine Biological Laboratory, Woods Hole, MA, USA
[3]Department of Molecular Biology, Princeton University, Princeton, NJ, USA
[4]Lewis-Sigler Institute for Integrative Genomics, Princeton University, Princeton, NJ, USA

Abstract

Crowding increases the tendency of macromolecules to aggregate and phase separate, and regulated crowding contributes to subcellular organization and stress response. To explore the effect of crowding in a well-characterized model cytoplasm we developed methods to concentrate the macromolecule components of *Xenopus* egg extracts without changing small molecules. Egg cytoplasm contains a high concentration of glycogen that serves as an energy store for early development. When crowding was increased 1.4x, the egg cytoplasm de-mixed into two liquid phases of approximately equal volume, one of which was highly enriched in glycogen. Glycogen hydrolysis prevented and reversed de-mixing. Quantitative proteomics showed that the glycogen-rich phase was enriched in proteins that bind glycogen, participate in carbohydrate metabolism, or are part of very high molecular weight complexes. The glycogen-depleted phase was enriched in ribosomes, endoplasmic reticulum (ER) and mitochondria. Smaller soluble proteins were approximately equipartitioned. Glycogen is usually observed in aggregates in intact cells and recent work suggested a role for phase separation in its localization. Our results show that glycogen particles can spontaneously de-mix and suggest that de-mixing may be regulated by crowding.

Statement of Significance

Cytoplasm is often treated as an aqueous solution of proteins and RNA, but many cells also contain very high concentrations of energy storage polymers such as glycogen. This study shows that glycogen is not merely a passive, well mixed component. Rather, it can reorganize cytoplasm by driving liquid-liquid demixing under modestly increased crowding conditions. Crowding changes occur during growth, stress, osmotic shifts, and metabolic transitions, yet their effects on abundant cellular polymers are poorly understood. By showing that glycogen can form a distinct liquid phase that selectively recruits or excludes major cellular components, this work identifies a simple physical mechanism for glycogen aggregation and resulting cytoplasmic re-organization. Glycogen localizes to dense aggregates in liver and muscle, but the

aggregation principle was unknown. This work suggests that demixing occurs under crowded conditions and could be relevant to normal organization of glycogen-rich tissues such as liver and muscle, and potentially to diseases in which glycogen accumulates or mislocalizes.

Introduction

The concentration of macromolecules in cytoplasm is thought to reflect a balance between competing physicochemical effects. Increased concentrations tend to speed up biochemistry, but very high concentrations can cause excessive crowding, leading to deleterious interactions and potentially freezing macromolecular dissociation. Crowding tends to promote macromolecular assembly reactions, including linear polymerization and phase-separated condensate assembly [1]. Increasing crowding may contribute to a liquid-to-glass transition in bacterial and yeast cytoplasm under energy stress [2-4] or mechanical compression [5]. Whether this glass transition is a universal response to increased crowding is not known, though local dehydration was shown to decrease the mobility of macromolecules in human cells in tissue culture [6].

The concept of crowding is related to those of excluded volume effects [7] and colloid osmotic pressure [8-11]. Importantly, the ability of a molecule to exert crowding effects, and the response of molecules to crowding, depend on their size. Cytoplasm is polydisperse and soluble biomolecules cover orders of magnitude in radius, spanning from water molecules to ribosomes and other large complexes. Increased crowding tends to preferentially affect larger molecules because they start to physically interact before smaller molecules [12]. This reduces the mobility of large molecules, such as ribosomes, at concentrations which still allow smaller molecules to move in the crevices between them [13]. One might expect increased crowding to induce demixing of the largest components while leaving smaller components free to diffuse, such as in polydisperse colloidal systems with depletion interactions [14]; however, the effect of crowding on cytoplasm is complicated by binding reactions, which may cause smaller molecules to demix along with larger ones to which they bind.

The storage polysaccharide glycogen is one of the most abundant macromolecules in many animal cells, on the order of 10% (w/w) in fed liver tissue [15, 16]; however, it is often forgotten in discussions of the structure and dynamics of cytoplasm. Glycogen is synthesized as a particle that consists of a highly branched, covalent polymer of glucose, usually initiated by polymerization from the surface of the nucleation protein glycogenin [16]. The glycogen-associated proteome includes enzymes involved in

glycogen synthesis or hydrolysis as well as regulatory proteins [17, 18]. Glycogen particles can be of different sizes, with a diameter of ~20 nm typical [19, 20]. Glycogen particles are highly soluble in water, though they can form higher order assemblies [16, 21]. Glycogen has long appeared as clustered granules in electron micrographs [22-24]. Recent reports have documented liquid-liquid phase separation of glycogen in liver cells [25] and in *Escherichia coli* [26]; however, the forces driving phase separation of glycogen in cytoplasm remain unclear.

Xenopus egg extracts provide a well-characterized model cytoplasm. They are prepared from eggs by centrifugal crushing with minimal dilution and maintain many of the biochemical and biophysical properties of native egg cytoplasm. Egg extracts contain ~80 mg/mL protein and ~80 mg/mL glycogen. The glycogen provides an energy store for the developing embryo and may also provide a crowding function that promotes assembly of nuclei [27] and mitotic spindle poles [28]. We set out to investigate the effect of changes in crowding on cytoskeleton dynamics in egg extract, but when we increased crowding by 1.4x or higher, we observed bulk demixing into two phases. Though not our initial focus, macromolecular crowding can promote segregative phase separation in biological systems [1], as in analogous aqueous two-phase systems [29]. Here, we report that the demixing we observed depends on glycogen and generates one phase that is highly glycogen-enriched. These observations probably do not model any normal egg biology, but they are informative concerning the physical properties of glycogen and its influence on those of the cytoplasm.

Results

Crowded *Xenopus* egg extracts exhibit liquid-liquid demixing

To selectively increase macromolecular crowding of components greater than 25-30 kDa in *Xenopus* egg extracts while minimally perturbing ionic strength, pH, and metabolite concentrations, we developed two methods, which gave similar results. In the first method, dry Sephadex G-25 gel filtration resin was added directly to extract and then removed a few minutes later by centrifugal filtration. As the resin swells, it absorbs water and small molecules, but macromolecules greater than 25 kDa are excluded and therefore become more crowded (Fig 1A). This method was convenient for small volumes of extract. The crowding factor depended on the amount of dry resin added per volume extract (Figs 1B, S1). In the second method, a 30 kDa MWCO centrifugal filter unit was used to concentrate macromolecules greater than 30 kDa. This method was convenient for larger volumes. The extent of macromolecule concentration was measured by adding a macromolecular fluorescent probe to the extract before concentration, such as Streptavidin

(53 kDa) fused to Alexa Fluor 647 (Fig 1C), then comparing the fluorescence intensity of a specimen of fixed depth before and after crowding by fluorescence microscopy with a low magnification objective (Fig S1).

When crowding was increased to 1.2x, the extract remained similar in appearance to uncrowded extracts, as observed in brightfield and fluorescence images (Fig 1B,C). At 1.4x-1.5x, the extract underwent spontaneous demixing over a few minutes at both 0 °C and 20 °C. This unexpected phenomenon was further characterized. At 1.9x macromolecules in the extract appeared to precipitate, and this regime was not examined further. At 1.4x-1.5x, demixing occurred throughout the sample and the two phases remained co-mingled in the tube. They had different densities and could be separated in bulk by centrifugation at 20000 rcf for 20 min. The denser phase had an index of refraction of 1.39, and the less dense phase 1.38 via Abbe refractometry, which has a nominal precision of 0.0002. This refractive index difference made demixing easy to follow by phase contrast or DIC microscopy. Both phases exhibited all the hallmarks of liquids, including deformation under flow, splitting, fusion, and rounding towards a spherical shape driven by surface tension [30] (Fig 1D, Video S1).

Figure 1. Crowded *Xenopus* egg extracts exhibit liquid-liquid demixing. (A) The macromolecular fraction greater than 25 kDa of *Xenopus* egg extracts was crowded by adding dry Sephadex G-25 resin, which selectively imbibes water and small molecules as it swells. (B) Brightfield images. Above 1.4x crowding, the extract remained liquid-like and exhibited patches with different light scattering properties. Above 1.9x crowding, precipitation occurred. (C) The crowding factor was estimated by quantification of fluorescence of a protein probe greater than 25 kDa added before crowding, in this case Streptavidin (53 kDa) fused to Alexa Fluor 647. The Streptavidin-A647 partitioned into one of the phases. Crowding factors estimated from lower magnification images in Fig S1. (D) Timelapse differential interference contrast (DIC) images of a 1.4x crowded extract confined between coverslips. The phases exhibited hallmarks of liquids, including deformation under transient flow after confining the crowded extract between the coverslips, splitting, fusion, and rounding by surface tension. Video S1 shows many examples of these dynamics.

Role of glycogen in demixing

As a hint to the composition of the denser phase, its higher refractive index suggested a higher concentration of glycogen, which has a higher density and refractive index than protein. We measured the glycogen concentration in unperturbed extract and the two phases using an assay that digested it to glucose for colorimetric quantification. Glycogen was highly enriched in the denser phase (Fig 2A). The glycogen concentration was 80 ± 5 mg/mL in uncrowded extracts, 15 ± 6 mg/mL in the less dense phase, and 295 ± 56 mg/mL in the denser phase (Fig 2A) (Methods).

To test for a role of glycogen in demixing, we hydrolyzed it using the enzyme amyloglucosidase (AG). Glycogen digestion by AG blocked demixing when added before crowding (not shown) and reversed it when added after crowding (Fig 2B). We concluded that demixing depends on intact glycogen.

Figure 2. In crowded extracts, glycogen partitions between the phases and is necessary for phase separation. (A) Glycogen highly partitioned between the phases, as measured by a colorimetric assay. In uncrowded extracts (Crude), the concentration of glycogen was 80 ± 5 mg/mL (N=3 biological replicates). In crowded extracts, the glycogen concentration was 15 ± 6 mg/mL in the less dense phase (Light) and 295 ± 56 mg/mL in the denser phase (Heavy) (N=3 biological replicates). (B) Crowded extracts exhibited demixing in DIC micrographs. Addition of amyloglucosidase (AG), which digests glycogen into glucose, caused the phases to dissolve and the system to return to a single phase, suggesting demixing requires intact glycogen.

Ultrastructure of glycogen-enriched (G) and -depleted (R) phases

To probe the ultrastructure and possible composition of the two phases, we performed thin-section electron microscopy with conventional heavy metal staining. Uncrowded extracts appeared mottled with uniformly distributed mitochondria and ER (Fig 3A). Crowded extracts exhibited two major phases as in optical micrographs (Fig 3B). One of the phases bound more of the uranium and lead ions used to generate contrast (Fig 3B). These heavy metals tend to bind proteins and nucleic acids. To identify the phases in electron micrographs, they were isolated in bulk by centrifugation then imaged separately (Methods). The glycogen-depleted phase (Fig 3C) was more heavily stained than the glycogen-enriched phase (Fig 3D). Mitochondria concentrated at the interface between the phases (Fig 3B,E) and were also present within the glycogen-depleted phase (Fig 3C). The more densely stained, glycogen-depleted phase was textured with structures ~25 nm in diameter, which we interpret as ribosomes (Fig 3E''). Ribosomes are abundant in *Xenopus* eggs and are mostly present as dormant 80S particles stabilized by hibernation proteins [31]. Enrichment of ribosomes in the non-glycogen phase was confirmed by proteomics (see below). Hereafter, we refer to the glycogen-depleted phase as "R" for ribosomes and the glycogen-enriched phase as "G" for glycogen.

Figure 3. Ultrastructure of glycogen-enriched (G) and -depleted (R) phases. (A) Uncrowded extract did not exhibit bulk demixing but exhibited a mottled appearance. Scale bar applies to panels A-D. (B) Crowded extracts exhibited bulk demixing, with one phase more strongly stained by heavy metals than the other. (C,D) The glycogen-depleted and glycogen-enriched phases were isolated from one another in bulk by centrifugation and imaged separately. The glycogen-depleted phase was more stained than the glycogen-enriched phase. (E) Mitochondria often localized along the interface between the phases or in the higher contrast phase. E is a different micrograph than B. E' is a zoom of the white box in panel E, and E'' is a zoom of the white box in panel E'. The strongly stained phase had a granular appearance with features ~25 nm in diameter, which we interpret as ribosomes.

Partition of fluorescent probes between G and R phases

To observe partitioning of macromolecules between the phases, we next pursued fluorescence microscopy. Fluorescent probes such as EB1-mApple (57 kDa) and Streptavidin (53 kDa) labeled with Alexa Fluor 647 were added to crowded extracts. Then, to estimate partitioning of each probe between the phases, the G and R phases were isolated from one another in bulk by centrifugation (Methods). We could thus measure the relative intensities of the fluorescent probes (Fig 4A,B), as well as identify the mixed phases using the fluorescent probes (Fig 4C). Relative fluorescence intensities in the phases scored by

microscopy were similar to bulk partition coefficients (Fig 4D). Among the fluorescent probes imaged, EB1-GFP (57 kDa), Fab fragment antibody (50 kDa) labeled with Alexa Fluor 647, and 70 kDa dextran-Alexa Fluor 488 partitioned preferentially into the R phase (Fig 4E-G, I-J). Glycogen phosphorylase A (PYGL, 188 kDa as dimer), a glycogen-binding protein, labeled with Pacific Blue partitioned preferentially into the G phase (Fig 4K). Mitochondria imaged by NADH autofluorescence localized along the interface between phases (Fig 4H), as seen by electron micrographs (Fig 3B,E).

Figure 4. Fluorescent probes partitioned between G and R phases. (A) EB1-mApple and Streptavidin-A647 in G and R phases, isolated from one another in bulk by centrifugation. Samples were confined between coverslips, and the images show the interface between the samples (left) and the surrounding air (right). (B) Both probes partitioned preferentially into the R phase than the G phase. Intensity profiles were measured from left to right across the interface. (C) Mixed phases in crowded extract. (D) Intensity profile along the black dotted lines overlaid on panel C. The relative intensities of the mixed phases (maximum vs minimum values in panel D) were similar to the relative intensities of the isolated phases (solid vs dashed values in panel B). (E-H) EB1-GFP and Fab-Alexa Fluor 647 likewise partitioned preferentially into the R phase, while mitochondria imaged by NADH autofluorescence localized along the interface between phases, as seen by electron micrographs. (I-K) 70 kDa dextran-Alexa Fluor 488 partitioned into the R phase, while PYGL-Pacific Blue partitioned into the G phase.

Quantitative proteomic analysis of G and R phases

To quantify the proteomes of the G and R phases, we performed multiplexed mass spectrometry analysis using the MultiNotch MS3 method [32-34]. For this analysis, we compared both the Sephadex G-25 resin or 30 kDa MWCO centrifugal filter unit methods for concentration. Results were similar for the two methods (Fig S2, Table S1). Fig 5 reports measurements averaged across the two methods and several repeats.

Known glycogen-binding proteins selectively partitioned into the G phase, with log base 2 partition coefficients of 1-3 (Fig 5A). These values approach the partition coefficient of glycogen itself (Fig 2A). Enzymes involved in carbohydrate metabolism also partitioned into the G phase, though with lower partition coefficients than proteins known to bind glycogen (Fig 5A). Ribosomal subunits, ER and mitochondrial proteins selectively partitioned into the R phase (Fig 5A), consistent with the electron micrographs (Fig 3C,E).

Native molecular weight appeared to play a role in partitioning. Several of the highest native MW protein complexes other than ribosomes partitioned into the G phase, such as major vault protein (MVP, 13 MDa), ferritin (FTH1, 450 kDa), chaperonin-containing T-complex (CCT, 960 kDa), and the 26S proteasome (PSMA, 2 MDa) (Fig 5A). We then plotted log base 2 partition coefficients with respect to native MW (Fig 5B), based on previous estimates of native MW with an upper bound of 256 kDa [35]. Proteins with native

MW smaller than 100 kDa had a slight preference for the G phase, with average log base 2 partition coefficient 0.4 ± 0.8 (Fig 5C). In contrast, most proteins with native MW greater than 256 kDa partitioned into the R phase, with average log base 2 partition coefficient -1.3 ± 1.6 (Fig 5C). These data suggest that the G phase is less crowded, so it has more space to accommodate large complexes. This effect may be offset by molecular interactions which recruit ribosomes and other complexes into the R phase.

Figure 5. Proteomics analysis suggests partitioning depends on binding and native MW. (A) Log base 2 partition coefficients of proteins sorted by Gene Ontology terms. Gray lines represent median values, boxes represent first and third quartile values, whiskers show the range of the data up to 1.5x the interquartile range, and circles represent outliers. (B) Log base 2 partition coefficients with respect to native MW less than 256 kDa. (C) Log base 2 partition coefficients of all proteins in complexes with native MW less than 100 kDa or greater than 256 kDa. Replicates in Figure S2.

Discussion

When macromolecular crowding of *Xenopus* egg extracts was increased 1.4x over control, we observed glycogen-dependent demixing into liquid phases, with one phase highly enriched in glycogen. This is the first observation of glycogen-dependent demixing in a physiologically relevant system. In vitro systems facilitate biochemical control, but previous in vitro studies characterized solutions of purified glycogen and artificial crowders such as polyethylene glycol [25, 26]. In reconstituted systems, the size, concentration, and chemical properties of macromolecular crowders have significant effects on protein association and phase separation [7]. Regarding the crowding factor at which demixing occurred in our system, given that macromolecules account for the majority of the dry volume, the crowding factor approximately equals the change in the dry volume fraction. Uncrowded *Xenopus* extracts have a protein concentration of approximately 95 mg/mL, corresponding to a volume fraction of approximately 7-10% [9]. We measured a comparable glycogen concentration of approximately 80 mg/mL in uncrowded extracts (Fig 2A). Assuming the volume fraction approximately scales with the concentration, we estimate protein plus glycogen may occupy 13-18% of the cytoplasmic volume. Then, at a crowding factor of 1.4x, the volume fraction of protein plus glycogen would be approximately 18-25%. We note that these estimates ignore both the volume occupied by organelles as well as protein sequestration in organelles and assembly in complexes [9]. In colloidal systems, changes of this magnitude in the dry volume fraction can induce phase separation, depending on the relative size of the colloids and depletants [36].

Both classic and newer evidence are consistent with a role of spontaneous demixing in locally concentrating glycogen withing cells. The high glycogen concentration in egg cytoplasm is comparable to that in hepatocytes from fed liver [15, 16], so our system is potentially relevant to other cell types.

Glycogen particles usually appear as aggregates in animal tissues [22-24, 37-39] and chloroplasts [40, 41]. Fawcett (1981) summarized extensive EM studies as showing that "glycogen is seldom uniformly distributed in the cytoplasm but tends to accumulate in dense regional deposits" [42]. Despite the commonly observed aggregation of glycogen, the forces driving aggregation were previously unknown. There is no published evidence for transport of glycogen by motor proteins, and its sheer abundance favors a spontaneous physical mechanism for aggregation.

Recent evidence is consistent with phase separation and spontaneous demixing of glycogen particles. Glycogen was proposed to undergo phase separation in cultured HepG2 liver cells overexpressing a constitutively active mutant of glycogen synthase [25]. That study also described fluorescence recovery consistent with liquid behavior after photobleaching (FRAP) of a starch-binding protein domain fused to GFP (CBM20-GFP), though recovery could in part reflect binding and unbinding of the noncovalent probe. Liu et al. proposed that glycogen aggregation is a causal factor in the initiation of liver cancer [25], which suggests medical significance of our observations. In cultured astrocytes, glycogen labeled covalently with the fluorescent glucose derivative 2-NBDG exhibited heterogenous localization [43]. In *Escherichia coli* transitioning from exponential to stationary phase, glycogen condensates excluded cytoplasmic proteins and nucleoids [26]. This study performed atomic force microscopy (AFM) and observed the glycogen condensates had a stiffness comparable to that of liquid cytoplasm and lower than that of solid protein aggregates [26].

Proteomic analysis suggested that partitioning of proteins between our G and R phases depends on both molecular interactions that promote affinity and native MW, which makes proteins and complexes differentially sensitive to crowding. Specific binding interactions presumably caused glycogen-binding proteins to partition preferentially into the G phase with an average partition coefficient similar to that of glycogen itself (Fig 5A). Enzymes involved in carbohydrate metabolism also partitioned into the G phase (Fig 5A). These spanned a range of native MWs from 33 to 241 kDa, with no apparent correlation between partition coefficient and native MW (Table S1). Some of these have been shown to weakly bind glycogen in an adipocyte glycogen proteome [17, 18]. Association between glycolytic enzymes has also been reported, but its functional significance remains unclear [44]. Electrostatics were recently shown to generate interactions between macromolecules in *Xenopus* egg extract [45], and both electrostatic and hydrophobic interactions affect protein association in cells [46]. While transient and nonspecific, these might be of sufficient energy to contribute to phase partitioning in our system. Consistent with a role for

native MW, the G phase enriched several especially large protein complexes not known to bind glycogen [17, 18] (Fig 5A). A role for native MW in partitioning could suggest that physical demixing, related to depletion forces in colloidal systems, may contribute to high local concentrations of glycogen; however, we cannot rule out other mechanisms including binding interactions between glycogen particles and local concentration of biosynthetic enzymes. Relative contributions of entropic and binding considerations may be considered within excluded volume theory [7].

Glycogen-dependent demixing of frog egg cytoplasm provides a new perspective on how bulk physical behavior can help organize the complex mixture that comprises cytoplasm. Frog eggs evolved in a freshwater environment and are not known to exhibit desiccation resistance, so the demixing we observed is unlikely to be of direct physiological relevance. However, it provides the first direct evidence that glycogen particles can locally concentrate by spontaneous demixing. This observation may be broadly relevant to the biology of glycogen, as discussed above. Cytoplasm is a remarkable substance and much remains to be discovered concerning its physical properties. *Xenopus* egg extracts remain an important system for such inquiry, as shown by this study and recent work on electrostatic interactions between mobile macromolecules [45].

Materials and Methods

Preparation of Xenopus egg extracts

Xenopus egg extracts were prepared as described previously [47]. Most experiments used extracts prepared with Cytochalasin D to prevent F-actin polymerization, in which case 100 µg/mL Cytochalasin D was added before the crushing spin at 18 °C, and 10 µg/mL Cytochalasin D was added after the crushing spin. Extracts with intact F-actin also demixed at similar crowding factors.

Crowding of Xenopus egg extracts

Xenopus egg extracts were crowded by two methods, using Sephadex G-25 resin or 30 kDa MWCO filter units, which gave similar results. To crowd using coarse Sephadex G-25 gel filtration resin (Sigma-Aldrich #GE17-0034-01), 30 µg dry resin was added to 150 µL extracts in a PCR tube. The resin was submerged and dispersed with a pipette tip, then the slurry was incubated for 5 min on ice. Then several holes were punched in the bottom of the PCR tube using the tip of a 27G needle, which makes holes small enough to retain resin in the tube. Then the PCR tube was placed inside a 0.5 mL tube, which was in turn placed inside a 1.5 mL tube for centrifugation. The tubes were centrifuged at 4000 rcf for 4 min to collect the

crowded extract in the 0.5 mL tubes. To crowd using filter units, extracts were centrifuged in Amicon filter units with 30 kDa MWCO (Millipore #UFC5030BK). Crowded extracts were then stored on ice. To estimate crowding factors, macromolecular fluorescent probes were added to extracts before crowding.

Fluorescent probes

To observe the two phases and estimate partitioning of fluorescent probes, we imaged Fab fragment antibody labeled with Alexa Fluor 647 (Jackson ImmunoResearch #111-607-003), Streptavidin labeled with Alexa Fluor 647 (Jackson ImmunoResearch #016-600-084), and Phosphorylase A (Sigma-Aldrich #P1261) labeled with Pacific Blue (Thermo Fisher #P10163).

Digestion of glycogen

Amyloglucosidase (AG) (Sigma-Aldrich #A7420) was added to extracts to a final concentration of 1.25 mg/mL (8.7 µM).

Measurement of glycogen concentration

The glycogen concentration was measured by a colorimetric assay based on the peroxidase sensitive dye 3,3',5,5'-tetramethylbenzidine (TMB) (Sigma-Aldrich #860336). Glycogen was digested to glucose using amyloglucosidase (AG), then hydrogen peroxide was generated from glucose using glucose oxidase (Sigma-Aldrich #G7016), then TMB was oxidized to TMB diimine by the hydrogen peroxide with horseradish peroxidase (Sigma-Aldrich #P6782). In particular, reactions included 100 µg/mL TMB, 250 µg/mL AG, 250 µg/mL GO, 125 µg/mL HRP in 100 mM sodium citrate pH 5.0. Extracts and glycogen standards were titrated into reactions, and the TMB diimine absorbance at 660 nm was measured on a Synergy H1 plate reader (BioTek).

Measurement of protein concentration

Protein concentration in each phase was measured by Micro BCA following TCA precipitation.

Isolation of phases by centrifugation

Crowded extracts were centrifuged at 20000 rcf for 20 min. After centrifugation, the less dense R phase was aspirated into an 18 G blunt needle, carefully as not to disturb the interface between the R and G phases. The R phase appeared as two opaque layers of slightly different colors and both these were included in the R sample. Then a hole was punched in the bottom of the tube, and by pressing the top of

the tube, the higher density G phase was pushed through the hole, likewise carefully as to avoid the interface between the phases.

Electron microscopy

Extract was spread on coverslips then samples were prepared by standard methods. Extract samples were fixed with 1.5% glutaraldehyde in 0.1 M cacodylate buffer pH 7.4, post fixed with 1% osmium tetroxide/potassium ferrocyanide, en block stained with 1% uranyl acetate, dehydrated and embedded in Epon Araldite, then sectioned and on grid stained with uranyl acetate and lead citrate. Samples were viewed on a Tecnai G-2 BioTwin electron microscope and imaged with an AMT CCD camera.

Mass spectrometry

Samples were prepared following the MultiNotch MS3 method as described [32-34]. Briefly, samples were denatured in 5 M guanidine thiocyanate then reduced with 5 mM dithiothreitol (DTT) (US Biological #D8070) at pH 8.3 for 20 min at 60 °C. Samples were shifted to pH 7.4 then cysteines were alkylated with 20 mM N-ethylmaleimide (NEM) (from 1 M NEM stock in acetonitrile) for 30 min at room temperature, then an additional 10 mM DTT was added and samples were incubated for 10 min at room temperature. The eluate was precipitated with methanol/chloroform: starting with 100 µL eluate, we added 400 µL methanol, vortexed, 200 µL chloroform, vortexed, 300 µL water, and vortexed. Samples were centrifuged at 20000 rcf for 2 min, then the upper layer was discarded. We added 300 µL methanol, vortexed, and centrifuged at 20000 rcf for 2 min. All liquid was aspirated, then we added 500 µL chloroform, vortexed, 500 µL methanol, vortexed, and centrifuged at 20000 rcf for 2 min. All liquid was aspirated, and the pellet was partially air dried at room temperature. The pellet was resuspended in 8 M guanidine hydrochloride prewarmed to 60 C, then 20 mM HEPBS pH 9 was added to 5-10% (v/v), and the sample was incubated for approximately 30 min at 60 C, until fully dissolved. For the digestion, samples were diluted with 20 mM HEPBS pH 9 to 2 M guanidine hydrochloride, then LysC was added at 10 ng/mL or 1:100 LysC:lysate by mass (whichever larger), then incubated for 14 h at 37 C. Then samples were further diluted with 20 mM HEPBS pH 9 to 0.5 M guanidine hydrochloride, then 10 ng/µL LysC and 5 ng/µL Trypsin were added, then incubated for 8 h at 37 C. Samples were dried by SpeedVac then checked to confirm the absence of white particulates that can clog the column, especially in the samples derived from the glycogen-enriched phase. Then samples were labeled with TMTs: 100 µg protein was resuspended in 100 µL of 300 mM EPPS pH 8, then 20 µL TMT stock solution (20 µg/µL in acetonitrile) was added. Samples were vortexed, briefly centrifuged, then incubated for 2 h at room temperature. Reactions were quenched with 10 µL of 5%

hydroxylamine and incubated for 15 min at room temperature. Samples were desalted on a C18 column, resuspended in 1% formic acid, and measured by the MultiNotch MS3 method as described [32-34], with channels normalized by the total number of counts. Native MWs were based on previous estimates [35]. Gene Ontology terms used for Fig 5A were Glycogen binding: GO:0005978 (Glycogen biosynthetic process, BP) and GO:0005980 (Glycogen catabolic process, BP); Carbohydrate metabolism: GO:0005975 (Carbohydrate metabolic process, BP) excluding GO:0005978 (Glycogen biosynthetic process, BP), GO:0005980 (Glycogen catabolic process, BP), GO:0005739 (Mitochondrion, CC), and GO:0005759 (Mitochondrial matrix, CC); Ribosome: GO:0005840 (Ribosome, CC); ER: GO:0005783 (Endoplasmic reticulum, CC); and Mitochondria matrix: GO:0005759 (Mitochondrial matrix, CC) excluding GO:0005829 (Cytosol, CC).

Data availability

All data are available in the Supplementary Information of this article.

Author Contributions

JFP, CMF, and TJM designed and performed the research, analyzed the data, and wrote the original draft. MC prepared the electron micrographs for Fig 3. LR, MS, and MW conducted the quantitative proteomics measurements for Figs 5 and S2 and Table S1. All authors reviewed and edited the manuscript.

Declaration of Interests

The authors declare no competing interests.

Acknowledgements

This work was supported by NIH grants R35GM131753 (TJM) and R35GM128813 (MW), and MBL fellowships from the Evans Foundation, MBL Associates, and the Colwin Fund (TJM and CMF). JFP was supported by the Fannie and John Hertz Foundation, the Fakhri lab at MIT, the MIT Department of Physics, and the MIT Center for Bits and Atoms. The authors thank Keisuke Ishihara for critical feedback on the manuscript, the Nikon Imaging Center at Harvard Medical School and Nikon at MBL for imaging support, and the National Xenopus Resource at MBL for support. The EB1-GFP construct was a gift from Kevin Slep (UNC Chapel Hill, NC).

Declaration of Generative AI in the Writing Process

During the preparation of this work, the authors used ChatGPT to help draft the Statement of Significance and as one method to predict compartments of proteins in column D of Table S1. The authors reviewed and edited the output as needed and take full responsibility for the content of the published article.

References

1. Andre, A.A.M., and Spruijt, E. (2020). Liquid-liquid phase separation in crowded environments. Int J Mol Sci *21*.
2. Joyner, R.P., Tang, J.H., Helenius, J., Dultz, E., Brune, C., Holt, L.J., Huet, S., Muller, D.J., and Weis, K. (2016). A glucose-starvation response regulates the diffusion of macromolecules. Elife *5*, e09376.
3. Munder, M.C., Midtvedt, D., Franzmann, T., Nuske, E., Otto, O., Herbig, M., Ulbricht, E., Muller, P., Taubenberger, A., Maharana, S.*, et al.* (2016). A pH-driven transition of the cytoplasm from a fluid- to a solid-like state promotes entry into dormancy. Elife *5*, e09347.
4. Parry, B.R., Surovtsev, I.V., Cabeen, M.T., O'Hern, C.S., Dufresne, E.R., and Jacobs-Wagner, C. (2014). The bacterial cytoplasm has glass-like properties and is fluidized by metabolic activity. Cell *156*, 183-194.
5. Okumus, B., Landgraf, D., Lai, G.C., Bakshi, S., Arias-Castro, J.C., Yildiz, S., Huh, D., Fernandez-Lopez, R., Peterson, C.N., Toprak, E.*, et al.* (2016). Mechanical slowing-down of cytoplasmic diffusion allows in vivo counting of proteins in individual cells. Nat Commun *7*, 11641.
6. Charras, G.T., Mitchison, T.J., and Mahadevan, L. (2009). Animal cell hydraulics. J Cell Sci *122*, 3233-3241.
7. Rivas, G., and Minton, A.P. (2016). Macromolecular crowding in vitro, in vivo, and in between. Trends Biochem Sci *41*, 970-981.
8. Marenduzzo, D., Finan, K., and Cook, P.R. (2006). The depletion attraction: An underappreciated force driving cellular organization. J Cell Biol *175*, 681-686.
9. Mitchison, T.J. (2019). Colloid osmotic parameterization and measurement of subcellular crowding. Mol Biol Cell *30*, 173-180.
10. Parsegian, V.A., Rand, R.P., and Rau, D.C. (2000). Osmotic stress, crowding, preferential hydration, and binding: A comparison of perspectives. Proc Natl Acad Sci USA *97*, 3987-3992.
11. Rand, R.P., Parsegian, V.A., and Rau, D.C. (2000). Intracellular osmotic action. Cell Mol Life Sci *57*, 1018-1032.
12. Hwang, J., Kim, J., and Sung, B.J. (2016). Dynamics of highly polydisperse colloidal suspensions as a model system for bacterial cytoplasm. Phys Rev E *94*, 022614.
13. Delarue, M., Brittingham, G.P., Pfeffer, S., Surovtsev, I.V., Pinglay, S., Kennedy, K.J., Schaffer, M., Gutierrez, J.I., Sang, D., Poterewicz, G.*, et al.* (2018). mTORC1 controls phase separation and the biophysical properties of the cytoplasm by tuning crowding. Cell *174*, 338-349 e320.
14. Fairhurst, D.J. (1999). Polydispersity in colloidal phase transitions. Thesis. University of Edinburgh, Edinburgh, United Kingdom.
15. Dowler, V.B., and Mottram, V.H. (1918). The distribution of blood, glycogen and fat in the lobes of the liver. J Physiol *52*, 166-174.
16. Prats, C., Graham, T.E., and Shearer, J. (2018). The dynamic life of the glycogen granule. J Biol Chem *293*, 7089-7098.

17. Stapleton, D., Nelson, C., Parsawar, K., Flores-Opazo, M., McClain, D., and Parker, G. (2013). The 3T3-L1 adipocyte glycogen proteome. Proteome Sci *11*, 11.
18. Stapleton, D., Nelson, C., Parsawar, K., McClain, D., Gilbert-Wilson, R., Barker, E., Rudd, B., Brown, K., Hendrix, W., O'Donnell, P.*, et al.* (2010). Analysis of hepatic glycogen-associated proteins. Proteomics *10*, 2320-2329.
19. Ioan, C.E., Aberle, T., and Burchard, W. (1999). Solution properties of glycogen. 1. Dilute solutions. Macromolecules *32*, 7444-7453.
20. Ioan, C.E., Aberle, T., and Burchard, W. (1999). Solution properties of glycogen. 2. Semidilute solutions. Macromolecules *32*, 8655-8662.
21. Nawaz, A., Zhang, P., Li, E., Gilbert, R.G., and Sullivan, M.A. (2021). The importance of glycogen molecular structure for blood glucose control. iScience *24*, 101953.
22. Porter, K.R., and Bruni, C. (1959). An electron microscope study of the early effects of 3'-Me-DAB on rat liver cells. Cancer Res *19*, 997-1009.
23. Revel, J.P., Napolitano, L., and Fawcett, D.W. (1960). Identification of glycogen in electron micrographs of thin tissue sections. J Biophys Biochem Cytol *8*, 575-589.
24. Revel, J.P. (1964). Electron microscopy of glycogen. J Histochem Cytochem *12*, 104-114.
25. Liu, Q., Li, J., Zhang, W., Xiao, C., Zhang, S., Nian, C., Li, J., Su, D., Chen, L., Zhao, Q., Shao, H., Zhao, H., Chen, Q., Li, Y., Geng, J., Hong, L., Lin, S., Wu, Q., Deng, X., Ke, R., Ding, J., Johnson, R.L., Liu, X., Chen, L., Zhou, D. (2021). Glycogen accumulation and phase separation drives liver tumor initiation. Cell *184*, 5559-5576.
26. Thappeta, Y., Cañas-Duarte, S.J., Wang, H., Kallem, T., Fragasso, A., Xiang, Y., Gray, W., Lee, C., Hardo, G., Cegelski, L., Jacobs-Wagner, C. (2025). Glycogen phase-separation drives macromolecular rearrangement and asymmetric division in *E. coli*. EMBO J *44*, 7434–7476.
27. Hartl, P., Olson, E., Dang, T., and Forbes, D.J. (1994). Nuclear assembly with lambda DNA in fractionated *Xenopus* egg extracts: an unexpected role for glycogen in formation of a higher order chromatin intermediate. J Cell Biol *124*, 235-248.
28. Groen, A.C., Coughlin, M., and Mitchison, T.J. (2011). Microtubule assembly in meiotic extract requires glycogen. Mol Biol Cell *22*, 3139-3151.
29. Walter, H., and Brooks, D. E. (1995). Phase separation in cytoplasm, due to macromolecular crowding, is the basis for microcompartmentation. FEBS letters *361*, 135-139.
30. Hyman, A.A., Weber, C.A., and Julicher, F. (2014). Liquid-liquid phase separation in biology. Annu Rev Cell Dev Biol *30*, 39-58.
31. Leesch, F., Lorenzo-Orts, L., Pribitzer, C., Grishkovskaya, I., Roehsner, J., Chugunova, A., Matzinger, M., Roitinger, E., Belačić, K., Kandolf, S., Lin, T.Y., Mechtler, K., Meinhart, A., Haselbach, D., Pauli, A. (2023). A molecular network of conserved factors keeps ribosomes dormant in the egg. Nature *613*, 712-720.
32. McAlister, G.C., Nusinow, D.P., Jedrychowski, M.P., Wuhr, M., Huttlin, E.L., Erickson, B.K., Rad, R., Haas, W., and Gygi, S.P. (2014). MultiNotch MS3 enables accurate, sensitive, and multiplexed detection of differential expression across cancer cell line proteomes. Anal Chem *86*, 7150-7158.
33. Gupta, M., Sonnett, M., Ryazanova, L., Presler, M., and Wuhr, M. (2018). Quantitative proteomics of Xenopus embryos I, Sample preparation. Methods Mol Biol *1865*, 175-194.
34. Sonnett, M., Gupta, M., Nguyen, T., and Wuhr, M. (2018). Quantitative proteomics for Xenopus embryos II, Data analysis. Methods Mol Biol *1865*, 195-215.
35. Wühr, M., Guttler, T., Peshkin, L., McAlister, G.C., Sonnett, M., Ishihara, K., Groen, A.C., Presler, M., Erickson, B.K., Mitchison, T.J.*, et al.* (2015). The nuclear proteome of a vertebrate. Curr Biol *25*, 2663-2671.

36. Dijkstra, M., Brader, J. M., & Evans, R. (1999). Phase behaviour and structure of model colloid-polymer mixtures. Journal of Physics: Condensed Matter *11*, 10079-10106.
37. Sheldon, H., Silverberg, M., and Kerner, I. (1962). On the differing appearance of intranuclear and cytoplasmic glycogen in liver cells in glycogen storage disease. J Cell Biol *13*, 468-473.
38. Coimbra, A., and Leblond, C.P. (1966). Sites of glycogen synthesis in rat liver cells as shown by electron microscope radioautography after administration of glucose-H3. J Cell Biol *30*, 151-175.
39. Galavazi, G. (1971). Identification of helical polyribosomes in sections of mature skeletal muscle fibers. Z Zellforsch Mikrosk Anat *121*, 531-547.
40. Crumpton-Taylor, M., Grandison, S., Png, K.M., Bushby, A.J., and Smith, A.M. (2012). Control of starch granule numbers in *Arabidopsis* chloroplasts. Plant Physiol *158*, 905-916.
41. Kasperbauer, M.J., and Hamilton, J.L. (1984). Chloroplast structure and starch grain accumulation in leaves that received different red and far-red levels during development. Plant Physiol *74*, 967-970.
42. Fawcett, D.W. (1981). The Cell.
43. Zhu, Y., Fan, Z., Wang, R., Xie, R., Guo, H., Zhang, M., Guo, B., Sun, T., Zhang, H., Zhuo, L., Li, Y., Wu, S. (2020). Single-cell analysis for glycogen localization and metabolism in cultured astrocytes. Cell Mol Neurobiol *40*, 801-812.
44. Schmitt, D.L., and An, S. (2017). Spatial organization of metabolic enzyme complexes in cells. Biochemistry *56*, 3184-3196.
45. Choi, A.A., Zhou, C.Y., Tabo, A., Heald, R., Xu, K. (2024). Single-molecule diffusivity quantification in *Xenopus* egg extracts elucidates physicochemical properties of the cytoplasm. Proc Natl Acad Sci USA *121*, e2411402121.
46. Zuo, W., Huang, M.R., Schmitz, F., and Boersma, A.J. (2024). Probing electrostatic and hydrophobic associative interactions in cells. J Phys Chem B *128*, 10861-10869.
47. Field, C.M., Pelletier, J.F., and Mitchison, T.J. (2017). Xenopus extract approaches to studying microtubule organization and signaling in cytokinesis. Methods Cell Biol *137*, 395-435.